NSWC TR 82-385

A MODIFIED JACCHIA 1977 MODEL ATMOSPHERE AND ITS APPLICATION TO ORBIT DETERMINATION

BY A. D. PARKS

STRATEGIC SYSTEMS DEPARTMENT

MAY 1982

Approved for public release; distribution unlimited.

NAVAL SURFACE WEAPONS CENTER

Dahlgren, Virginia 22448 • Silver Spring, Maryland 20910

UNCLASSIFIED

SECURITY CLASSIFICATION OF THIS PAGE *(When Data Entered)*

REPORT DOCUMENTATION PAGE		READ INSTRUCTIONS BEFORE COMPLETING FORM
1. REPORT NUMBER NSWC TR 82-385	2. GOVT ACCESSION NO. A137921	3. RECIPIENT'S CATALOG NUMBER
4. TITLE *(and Subtitle)* A MODIFIED JACCHIA 1977 MODEL ATMOSPHERE AND ITS APPLICATION TO ORBIT DETERMINATION		5. TYPE OF REPORT & PERIOD COVERED Final
		6. PERFORMING ORG. REPORT NUMBER
7. AUTHOR(s) A. D. Parks		8. CONTRACT OR GRANT NUMBER(s)
9. PERFORMING ORGANIZATION NAME AND ADDRESS Naval Surface Weapons Center (K13) Dahlgren, VA 22448		10. PROGRAM ELEMENT, PROJECT, TASK AREA & WORK UNIT NUMBERS 63701B
11. CONTROLLING OFFICE NAME AND ADDRESS Defense Mapping Agency Washington, DC 20370		12. REPORT DATE May 1982
		13. NUMBER OF PAGES 39
14. MONITORING AGENCY NAME & ADDRESS*(if different from Controlling Office)*		15. SECURITY CLASS. *(of this report)* UNCLASSIFIED
		15a. DECLASSIFICATION/DOWNGRADING SCHEDULE

16. DISTRIBUTION STATEMENT *(of this Report)*

Approved for public release; distribution unlimited.

17. DISTRIBUTION STATEMENT *(of the abstract entered in Block 20, if different from Report)*

18. SUPPLEMENTARY NOTES

19. KEY WORDS *(Continue on reverse side if necessary and identify by block number)*

Jacchia-Bass model atmosphere
Orbit improvement programs

20. ABSTRACT *(Continue on reverse side if necessary and identify by block number)*

The NSWC modified version of the Jacchia-Bass model atmosphere is described. The feasibility of incorporating it into operational orbit improvement programs is discussed.

DD FORM 1 JAN 73 1473 EDITION OF 1 NOV 65 IS OBSOLETE
S/N 0102-LF-014-6601

UNCLASSIFIED

SECURITY CLASSIFICATION OF THIS PAGE *(When Data Entered)*

FOREWORD

This report has been prepared to present a description of the NSWC version of the Jacchia-Bass model atmosphere. Also presented are the results of a study which evaluated the model's performance when used to compute aerodynamic drag accelerations for low altitude earth satellites during orbit improvement processes. Recommendations are made concerning the utilization and implementation of this model atmosphere into orbit determination programs.

Released by:

O. F. BRAXTON, Head
Strategic Systems Department

CONTENTS

TABLES

ILLUSTRATIONS

ILLUSTRATIONS (Continued)

1.0 INTRODUCTION

The orbital motion of an artificial earth satellite is perturbed by an aerodynamic drag force, which results from its interaction with the atmosphere. The magnitude of this drag force is directly proportional to the local atmospheric density, which depends upon the time and satellite position in a very complicated way. The effects of aerodynamic drag upon satellite orbits are most important in the altitude region from 120 km to 400 km above the surface of the earth. Satellites with perigee altitudes below 120 km suffer such great deceleration that their lifetimes before reentry are so short as to be impractical. For satellites with perigee altitudes above 400 km the orbital perturbations induced by atmospheric drag are relatively small.

The region of the atmosphere above 120 km is called the thermosphere, and a number of thermospheric models have been developed in an attempt to represent its behavior. These models generally fall into one of two categories: theoretical models which strive to achieve a description of thermospheric behavior in terms of the associated basic physical processes, and empirical models, which attempt to provide thermospheric data by using computationally efficient methods.

One of the latest in a series of empirical thermospheric models is the Jacchia 1977[1] (J77) model atmosphere. Although empirical in nature, the J77 model atmosphere is quite complex and requires extensive computer storage space. As a result, it is not particularly well suited for many aerodynamic drag computation applications. The complexity and storage requirement of the J77 model have been markedly reduced recently by modifications introduced by J. B. Bass.[2,3] The Bass-modified J77 model will be referred to hereafter as the JB model atmosphere.

A copy of the JB model atmosphere was obtained by the author from the Air Force Geophysics Laboratory and its utility analyzed for implementation into orbit improvement programs developed and used at the Naval Surface Weapons Center (NSWC), Dahlgren, Virginia. It was determined that the JB model is not completely adequate structurally for direct implementation into such programs, principally because it does not compute the partial derivative of total atmospheric density with respect to altitude above the earth's surface (this quantity is required when integrating the variational equations in the NSWC programs). This prompted an NSWC modification of the JB model, hereafter referred to as the modified JB (MJB) model, to make it compatible with NSWC requirements.

This report has been prepared to provide an overview of the MJB model atmosphere, as well as discuss the methodology and results of a study performed to investigate the feasibility of implementing it into operational orbit improvement programs.

2.0 THERMOSPHERIC VARIATIONS MODELED BY THE MJB ATMOSPHERE

The following thermospheric variations are modeled by the MJB atmosphere:

a. Variation of composition and temperature with altitude
b. Variation with solar activity
c. Diurnal variation
d. Variation with geomagnetic activity
e. Semiannual variation
f. Seasonal-latitudinal variation

Each of these is discussed in the following subsections.

2.1 Variation of Composition and Temperature With Altitude

As altitude increases, photodissociation processes produce changes in the composition of the atmosphere. This results in a decrease of the molecular mass with height, primarily from replacement of molecular oxygen by atomic oxygen. At higher altitudes diffusive separation becomes dominant so that each individual gas is distributed with altitude according to its own molecular mass. Thus the abundance of lighter gases decreases less rapidly with height than that of the heavier gases, and above certain altitude thresholds the lighter gases predominate.

A basic feature of the structure of the thermosphere is a very steep temperature gradient in the altitude region between 90 km and 200 km. This occurs because of the absorption of solar radiation, particularly in the extreme ultraviolet portion of the spectrum. The absorbed radiation causes dissociation and ionization of atmospheric constituents with a consequent release of heat. The heat deposited in the atmosphere decreases with altitude for altitudes greater than 200 km, and the atmosphere approaches isothermality.

The atomic and molecular constituents modeled by the MJB atmosphere are O, O_2, N, N_2, He, Ar, and H. These are, of course, used to compute the total mass density. It should be mentioned that whereas the JB atmosphere models the density between 90 km and 2500 km, the MJB atmosphere models only the density above 125 km. This was done because NSWC is not currently associated with any satellite programs operating at altitudes less than 125 km. The introduction of this new lower altitude bound significantly reduced the storage requirements for the MJB atmosphere because the density and temperature profiles for this low altitude layer were strictly tabular in nature in the JB model.

A further reduction in the MJB storage was achieved by using the fact that the hydrogen density below 500 km is negligible and by employing the diffusive equilibrium equation for hydrogen for altitudes greater than or equal to 500 km. This facilitated the elimination of the extensive hydrogen density tables used by the JB model, while simultaneously providing an

analytically differentiable expression for the hydrogen density required to form the altitude partial of the total mass density.

2.2 Variation With Solar Activity

Solar ultraviolet radiation continuously interacts with the earth's upper atmosphere with a variable spectral intensity distribution that is dependent upon solar conditions. There are two components of this radiation that generate heat energy: day-to-day variations in the active regions on the solar disk and the more slowly varying component that is associated with the 11-yr solar cycle. The thermospheric density is strongly influenced by the changing levels of solar activity (and the resulting density variations effect aerodynamic drag on satellites).

The solar flux at 10.7-cm wavelength, $F_{10.7}$, is generally regarded as a readily available index of solar ultraviolet radiation. When the $F_{10.7}$ increases, there is an increase in the thermospheric temperature. In the MJB model the mean exospheric temperature is determined by a function of the daily $F_{10.7}$ (evaluated when one uses a time delay that depends upon local time), which reflects the effect of the daily varying component and a Gaussian weighted average of $F_{10.7}$, $\bar{F}_{10.7}$, (when one uses a time constant of 71 days) that represents the effect of the slowly varying components.

2.3 Diurnal Variation

There is a permanent thermal bulge in the atmosphere located in the sunlit hemisphere of the earth, which causes a day-to-night (diurnal) variation in the atmospheric density. The density peaks rather sharply around 1400 local solar time (LST); a nighttime minimum also exists and occurs around 0300 LST. The bulge also shifts with the seasons thus making the density a function of latitude as well.

The diurnal effect depends upon altitude. This dependence is a direct consequence of conduction heating. Below about 200 km the diurnal effect is barely detectable. In the 200- to 250-km altitude range the density is approximately 10 percent higher in the sunlight than the dark. At 400 km the day-to-night density ratio is about 1.5:1; at 600 km it is 6:1; and at 700 km it is more like 10:1 or greater.

2.4 Variation With Geomagnetic Activity

Geomagnetic storms usually occur when clouds of charged particles collide with the earth's magnetic field. These charged particles are believed to be ejected from the sun during the course of a solar flare. As a result, a large amount of solar radiation is emitted by the flare

region, which subsequently heats the earth's atmosphere. This heating mechanism is not well understood.

Variations with geomagnetic activity are characterized by the planetary geomagnetic index K_p and are divided into three categories. The first category is called the thermal component and is accounted for by an increase in temperature at all altitudes. The amount of atmospheric heating that causes this temperature increase is characterized by K_p evaluated at a time which allows for a delay due to the propagation time of the heating from the polar regions to the point of interest. This time delay varies inversely with magnetic latitude.

The second component is the effect of a change in the height of the homopause. The homopause is the level of transition between the homosphere* and the heterosphere.** This variation is accounted for by a correction to the individual number densities, which increase the abundance of Ar and O_2 while decreasing the abundance of O and He. No corrections are made to the N_2 or H number densities.

The third component is the equatorial wave, which describes a "piling up" of the atmosphere near the equator due to meridional flow driven by polar region heating. This latitude-dependent correction increases all constituents by the same fractional amount.

2.5 Semiannual Variation

The semiannual density variation is characterized by a primary density minimum in July followed by a high maximum in October, and a secondary minimum in January followed by a secondary maximum in April. The magnitude and altitude dependence of this variation changes considerably from solar cycle to solar cycle. Unfortunately the cause and mechanism of the variation are not well understood.

The MJB model accounts for the semiannual variation by modifying the density of all constituents by a factor that is a product of an altitude function and a function of day of the year.

2.6 Seasonal-Latitudinal Variation

The lower thermosphere is subject to a large seasonal-latitudinal variation in temperature and a smaller variation in density. The amplitude of the density variation increases very rapidly with height from 90 km up to a peak somewhere between 105 km and 120 km. It then decreases with altitude to 200 km where no such variation has been observed.

*The homosphere is the region of the atmosphere in which there is no gross change in composition, i.e., all the atmosphere up to about 100 km.

**The heterosphere is that upper portion of the atmosphere above the homosphere, which is characterized by variation in composition.

The MJB model adjusts each of the atmospheric constituents by an amount proportional to the product of solar declination and the sine of the latitude of the point of interest.

3.0 STUDY OBJECTIVES AND PROCEDURES

Numerical experiments were performed to provide data which, upon analysis, would determine the feasibility of implementing the MJB model atmosphere into operational orbit improvement programs developed and used by NSWC. The following subsections represent a discussion of the objectives to be achieved from the analysis of these data and the procedures used to perform the experiments.

3.1 Study Objectives

This study has been organized so that an understanding of the following can be obtained:

a. Complexity of the implementation of the MJB model atmosphere into NSWC orbit improvement programs
b. Ephemeris positional accuracies attained when the MJB and NSWC standard exponential atmospheres (SEA) are used for density computation in the ephemeris generation phase of the orbit improvement process
c. Doppler tracking data editing capabilities when the MJB and SEA models are used in the ephemeris generation process
d. Orbit improvement processing times when the MJB and SEA models are used in the ephemeris generation force model for density computation
e. Sensitivity of items (b) and (c) to variations in the solar flux

The standard exponential atmosphere mentioned above has been successfully used in NSWC orbit improvement programs for many years. The SEA atmospheric density is computed from the simple expression

$$\rho = e^{[c_1 h - c_2 - (c_3 h^2 + c_4 h - c_5)^{1/2}]}, \tag{3.1}$$

where h is the geocentric altitude of the satellite given by

$$h = r - \frac{a_e}{(1 + \frac{\epsilon^2}{1 - \epsilon^2} \sin^2 \phi)^{1/2}}, \tag{3.2}$$

and the quantities C_i (i = 1,2, ... , 5) are constants. In the last equation ϕ is the geocentric latitude, a_e is the earth's semimajor axis, ϵ is the earth's ellipticity, and r is the geocentric radial distance to the satellite.

It is apparent from the objectives enumerated above that the purpose of this study is to determine whether or not the highly simplified SEA model can be effectively replaced by the more sophisticated (but more cumbersome) MJB model.

3.2 Study Procedures

The MJB model atmosphere was introduced into a developmental version of the CELEST orbit determination program.[4] The actual implementation of the MJB code into CELEST was straightforward, the most difficult part being that needed to compute the peripheral information required by MJB, i.e., solar location and $F_{10.7}$, $\bar{F}_{10.7}$, and K_p. This version of CELEST also retained the SEA model so that the user could select either the MJB or SEA model by simply setting a control flag to the proper value. All subsequent numerical experimentation was conducted using this special version of CELEST, hereafter referred to as the SVOC.

The solar and geomagnetic conditions given in Table 3-1 and a synthetic gravity field of order 25 and degree 25 (hereafter denoted as 25 x 25) were used in the SVOC with MJB selected as the model atmosphere to generate a numerically integrated 24-hr earth-fixed trajectory. It was assumed that all the forces acting upon the satellite were perfectly modeled in this trajectory so that it represented the true path of the satellite; i.e., this was the "truth" trajectory for the satellite. This trajectory was used in the program SYNDAY to provide synthetic Doppler range difference tracking data. A 10-cm Gaussian noise level was introduced into the tracking data, as well as tropospheric refraction and signal transmission time corrections.

A series of test cases were generated, using the FILTER and CROSS-PASS FILTER sections of the SVOC (see Reference 4 for descriptions of these sections). Various combinations of the SEA and MJB model atmospheres and two gravity fields, the 25 x 25 and a synthetic field of order 14 and degree 14 (hereafter denoted as 14 x 14), were used to produce long arc station navigation solutions[6] which would provide information concerning the relative importance of drag and gravity induced ephemeris errors (the synthetic 14 x 14 field mentioned above is a truncated synthetic 25 x 25 field and has been shown to simulate realistic gravity errors relative to the 25 x 25 field for low-altitude satellite orbits). Test cases employing 4, 10, and 20 drag segments were also generated.

TABLE 3-1. SOLAR FLUX AND GEOMAGNETIC INDICES*

Day	$F_{10.7}$	$\bar{F}_{10.7}$	Time (GMT) 0	3	6	9	12	15	18	21	
298	100	100	3	4	2	4	3	1	2	3	
299	100	100	3	1	4	2	2	4	3	1	K_p
300	100	100	2	3	3	2	1	2	3	1	
301	100	100	1	2	2	1	2	2	2	1	

*The solar flux sensitivity test used the same K_p values but changed each of the $F_{10.7}$ and $\bar{F}_{10.7}$ to 200 flux units.

4.0 STUDY RESULTS

A total of 163 passes of synthetic tracking data were edited over a 64800-sec interval of time from trajectory epoch. The tangential (ΔT) and radial (ΔR) station navigation solutions obtained from the final iteration of the last processing cycle were plotted for each test case that was generated and the associated statistical information computed. The statistical data for each case generated, using the 25 x 25 gravity field, are given in Table 4-1. The statistical results for the 14 x 14 gravity field are given in Table 4-2. Also shown in these tables are processing times in (CPU) seconds per pass for each case. A compendium of radial and tangential station navigation error plots is presented in Appendix A (Figures A-1 through A-18).

The results of the editing performed by the cross-pass filter were examined and are presented in Figure 4-1. If for a given case the cross-pass filter determined that the navigation solutions for a pass were inconsistent with those for the remaining passes, then a vertical bar was drawn above the associated pass number delineated along the horizontal axis. It should be mentioned that no errors were introduced into the synthetic data that would produce rejection tags during the cross-pass editing process.

5.0 DISCUSSION AND CONCLUSIONS

A commentary based upon the results discussed in the previous section for each of the five objectives outlined in Section 3.1 is presented below in the same order of appearance as in that section:

(a) The experience derived from the implementation of the MJB model into the SVOC indicates that its implementation into a general version of PULSAR or CELEST should be straightforward. However, a somewhat complicated and unnatural method was employed for supplying solar flux and geomagnetic index data to the SVOC. A much more amenable method should be devised for supplying this data to the MJB model in a fully operational version of PULSAR or CELEST. One such method would be to automate the orbit determination programs to read the solar flux and geomagnetic data from a file containing these data that has been created and maintained by the GEOSOL file builder.[5]

(b) Examination of the data presented in the previous section demonstrates that, for satellites operating in special low-altitude orbits, the gravity induced errors are much more significant than those induced by atmospheric drag. In particular, the tangential and radial navigation errors induced by atmospheric drag are on the order of 10 m and 3 m, respectively. Those induced by an incomplete knowledge of the terrestrial gravity field in the tangential and radial directions are approximately 43 m and 20 m, respectively.

Further perusal of the statistical data presented in Tables 4-1 and 4-2 indicates that a significant fraction of the gravity errors can be absorbed by performing segmented fits to the drag coefficient. For the cases considered here, up to ~14 m and ~3 m of the gravity-induced errors have been absorbed in the tangential and radial directions, respectively, by using as many as 20 equilength drag segments during the fitting process. It is interesting to note that the introduction of drag segmentation into the fitting procedure appears to do little to remove the errors induced by atmospheric drag.

Finally, it should be mentioned that these data supply a quasi-realistic estimate of the size of the navigation errors that are to be expected for certain low-altitude orbits. Of particular interest are the tangential and radial errors of ~51 m and ~22 m, respectively, obtained in the single drag segment/SEA case when one uses the 14 x 14 gravity field. These should approxi-mate the magnitude of the errors encountered by the CROSS-PASS EDITOR of the PULSAR Doppler tracking data editor.[6]

(c) The results summarized in Figure 4-1 exhibit a fairly consistent cross-pass editing capability within a given gravity field. The cross-pass editing results obtained for the 14 x 14 field are similar regardless of the model atmosphere and number of drag segments used. A similar statement applies for the 25 x 25 gravity field. Of especial interest is the fact that the tagging within the 25 x 25 field is far less entropic than that within the 14 x 14 field. This apparent contrast in uniformity tends to emphasize again the relative dominance of the gravity field errors over those induced by atmospheric drag in the editing process.

TABLE 4-1. SUMMARY OF STATISTICAL RESULTS OBTAINED WHEN ONE USES A SYNTHETIC 25 x 25 GRAVITY FIELD

Atmosphere	Drag Segments	CPU Time Per Pass (sec)	Navigation Errors (m) ΔT Average	ΔT RMS	ΔT Sigma	ΔR Average	ΔR RMS	ΔR Sigma
MBJ	1	6.6	-0.3	3.6	3.6	-0.1	7.1	7.1
SEA	1	11.4	0.4	13.7	13.7	-2.3	10.4	10.2
SEA	4	11.7	0.4	12.7	12.7	-2.5	11.3	11.0

TABLE 4-2. SUMMARY OF STATISTICAL RESULTS OBTAINED WHEN ONE USES A SYNTHETIC 14 x 14 GRAVITY FIELD

Atmosphere	Drag Segments	CPU Time Per Pass (sec)	Navigation Errors (m) ΔT Average	ΔT RMS	ΔT Sigma	ΔR Average	ΔR RMS	ΔR Sigma
MJB	1	10.0	-1.3	46.4	46.6	4.1	23.5	23.2
SEA	1	8.4	1.7	50.8	50.9	2.0	22.2	22.2
MJB	4	11.0	-1.0	34.4	34.5	5.2	24.1	23.6
MJB	10	10.7	-2.3	36.1	36.2	5.6	24.4	23.8
MJB	20	10.8	-2.8	32.2	32.1	3.6	20.4	20.1
SEA*	1	6.3	3.0	56.9	57.0	-4.3	20.8	20.4

*$F_{10.7}$ = 200 Test Case Result

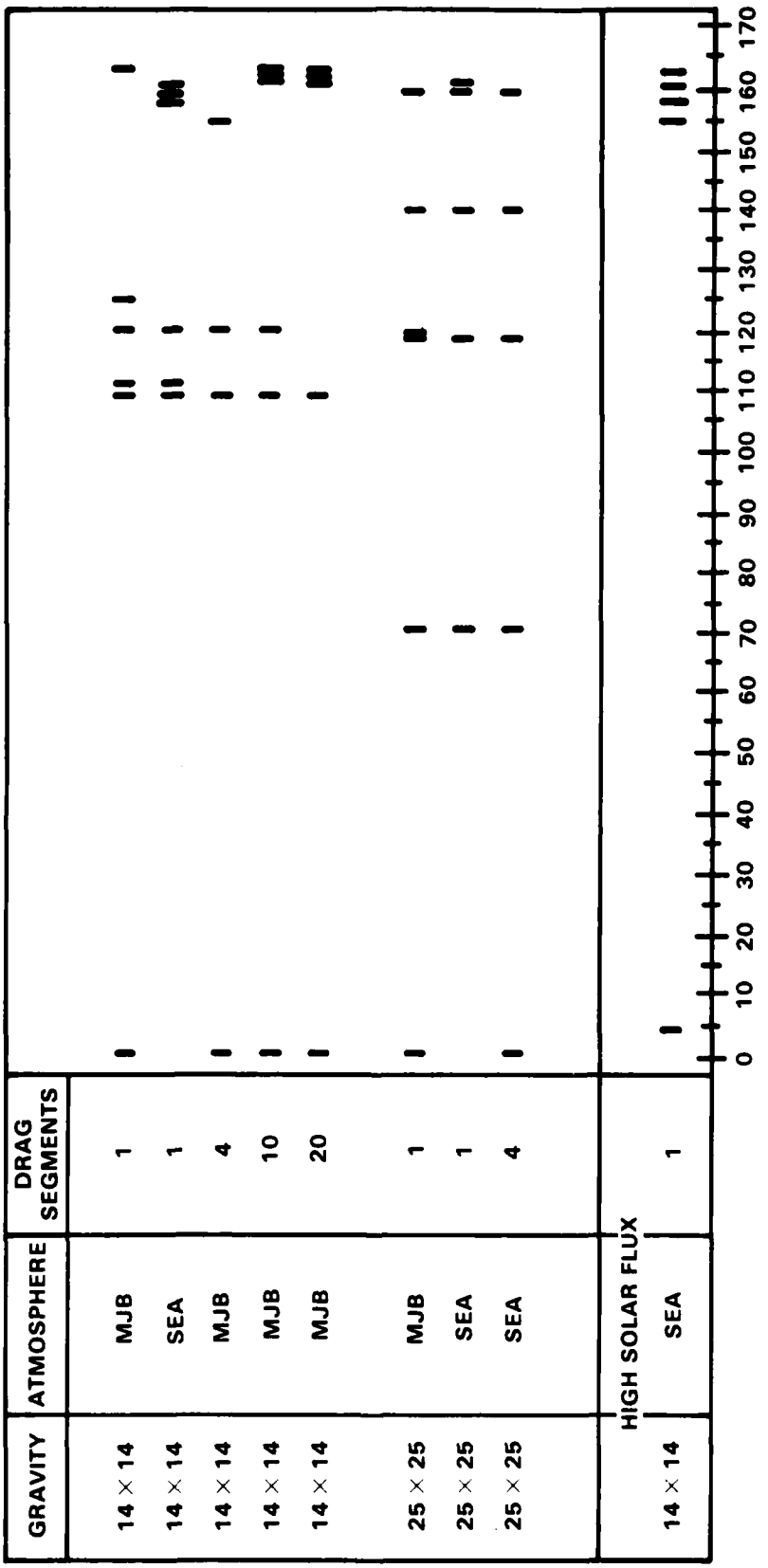

FIGURE 4-1. SUMMARY OF CROSS-PASS EDITING RESULTS

As was mentioned in a previous section, no errors were introduced into the synthetic tracking data that should produce rejection tags by the cross-pass editor. All passes that received rejection tags, except for the first, were low elevation passes for which a small change in the trajectory produced a significantly different tropospheric refraction correction. This resulted in a large radial dispersion and thus a rejection tag. The first pass was rejected for similar reasons because it was only a partial pass of 12 range difference measurements that were collected by the tracking station as the satellite was setting on the local horizon.

(d) The processing times per pass in CPU seconds are tabulated in Tables 4-1 and 4-2. Using the times needed to process the 14 x 14 gravity field cases, one finds that the use of the MJB model for density computations requires ~20 percent more CPU time than does the SEA model. A similar comparison cannot be made when one uses the 25 x 25 field, because, as expected, only one computational cycle was required for solution convergence in the single drag segment/MJB model test case. Two computational cycles were required for solution convergence for every other test case.

(e) The single high solar flux test case results tabulated in Table 4-2 provides an indication of the sensitivity of the editing process to the solar flux, as well as the relative inability of the SEA model to provide small ephemeris errors during periods of high solar activity. Although a slightly better radial navigation solution is obtained for the $F_{10.7}$ = 200 case, the tangential accuracy is further degraded by ~12 percent when the SEA model instead of the MJB model is used for density computation.

6.0 SUMMARY AND RECOMMENDATIONS

The preceding results and discussion have indicated that the highly sophisticated MJB model atmosphere can be used for drag deceleration computations in the orbit determination process with a moderate increase in processing time (i.e., ~19 percent) over that of the SEA model. However, for the orbital geometry considered in this analysis the gravity errors dominate the drag errors so that the gain in ephemeris accuracy is only slight during periods of low solar activity. A greater enhancement in ephemeris accuracy can be attained when the MJB model is used instead of the SEA model during periods of high solar activity. In keeping with these findings, the following recommendations are offered:

(a) Inplement the MJB model atmosphere into the NSWC versions of CELEST and PULSAR, retaining the SEA model. Provide a switch so that the user can select which atmosphere is to be used

(b) Automate the process of supplying solar flux and geomagnetic index data to the MJB model atmosphere by using the GEOSOL capability

(c) Using GEOSOL, accumulate and archive solar flux and geomagnetic data

(d) For better results during periods of high solar activity, use the MJB model atmosphere in orbit determination processing.

7.0 REFERENCES

1. L. G. Jacchia, *Thermospheric Temperature, Density, and Composition: New Models*, Smithsonian Astrophysical Observatory Special Report 375, Cambridge, Massachusetts, 1977.

2. J. N. Bass, *Condensed Storage of Diffusion Equation Solutions for Atmospheric Density Model Computations*, AFGL-TR-80-0038, Hanscom AFB, Massachusetts, 1980.

3. J. N. Bass, *Analytic Representation of the Jacchia 1977 Model Atmosphere*, AFGL-TR-80-0037, Hanscom AFB, Massachussetts, 1980.

4. J. W. O'Toole, *CELEST Computer Program for Computing Satellite Orbits*, NSWC TR-3565, Dahlgren, Virginia, 1976.

5. D. F. Walters, *Program Maintenance Manual for GEOSOL Data File and File Builder Program*, NSWC, Dahlgren, Virginia, 1982.

6. A. D. Parks, and T. I. Hicks, *A Mathematical Description of the PULSAR Doppler Tracking Data Editor*, NSWC TR 82-391, Dahlgren, Virginia, 1982.

APPENDIX A

STATION NAVIGATION ERRORS

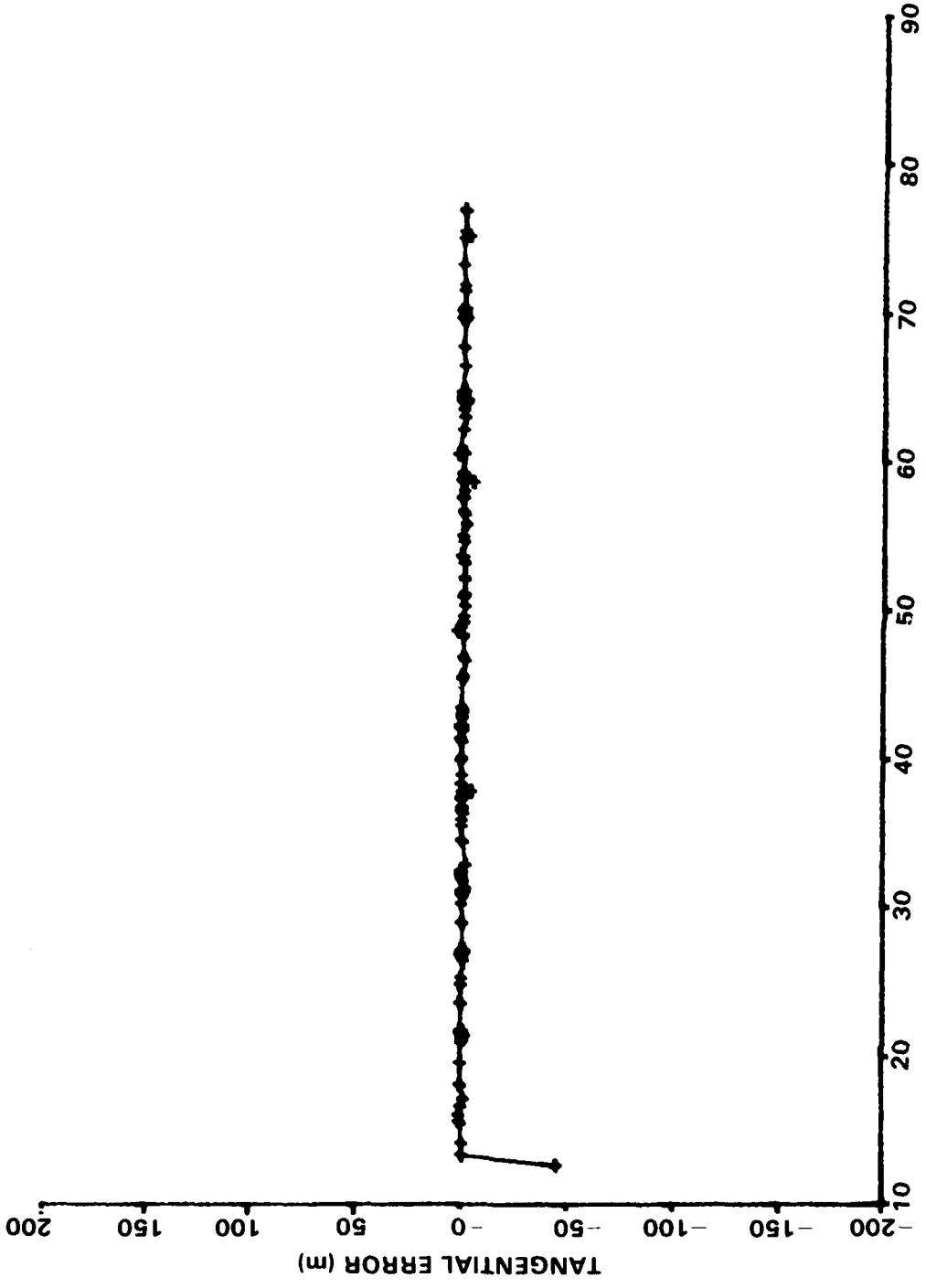

FIGURE A-1. 25 x 25 GRAVITY FIELD MJB MODEL ATMOSPHERE SINGLE DRAG SEGMENT

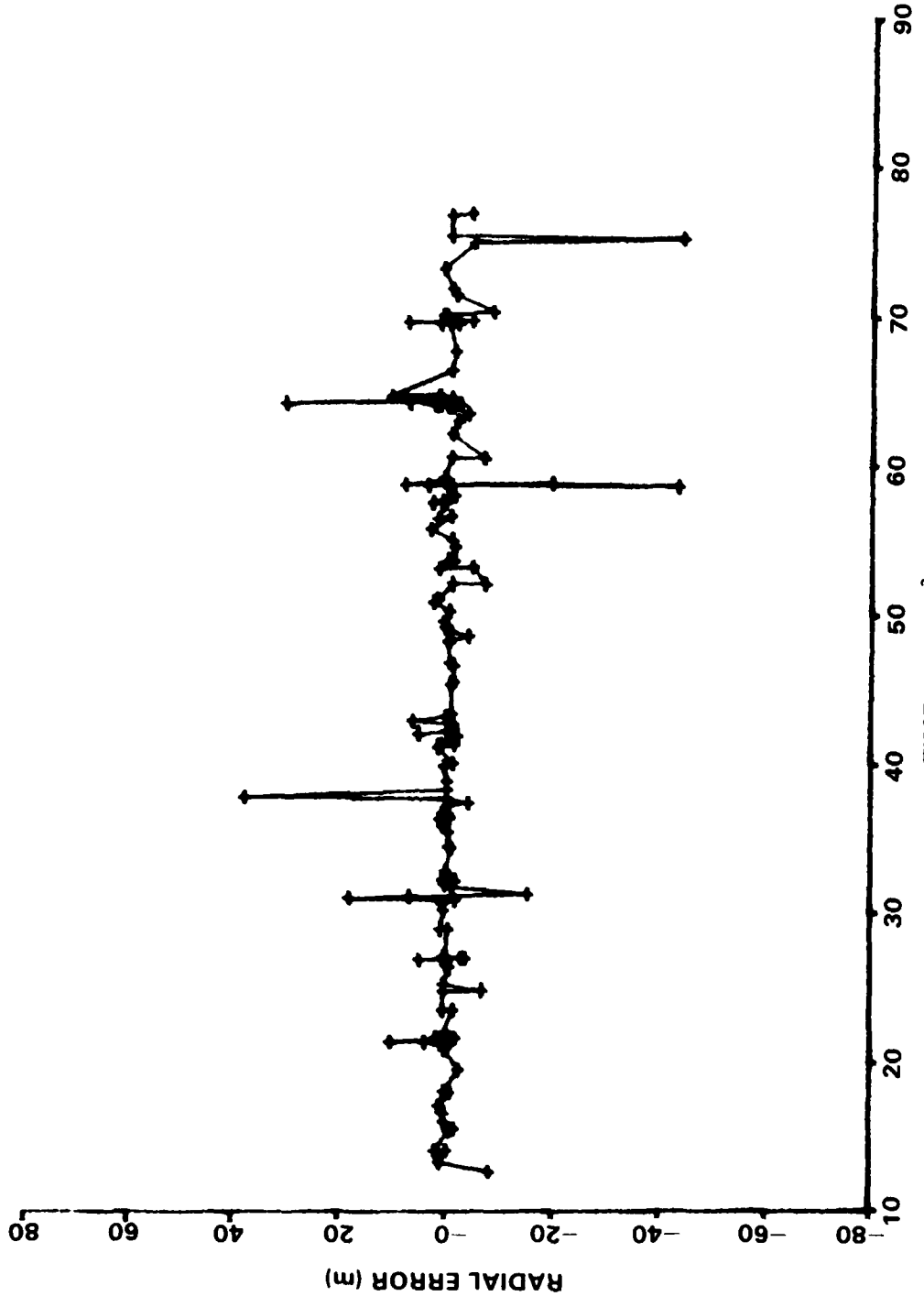

FIGURE A-2. 25 x 25 GRAVITY FIELD MJB MODEL ATMOSPHERE SINGLE DRAG SEGMENT

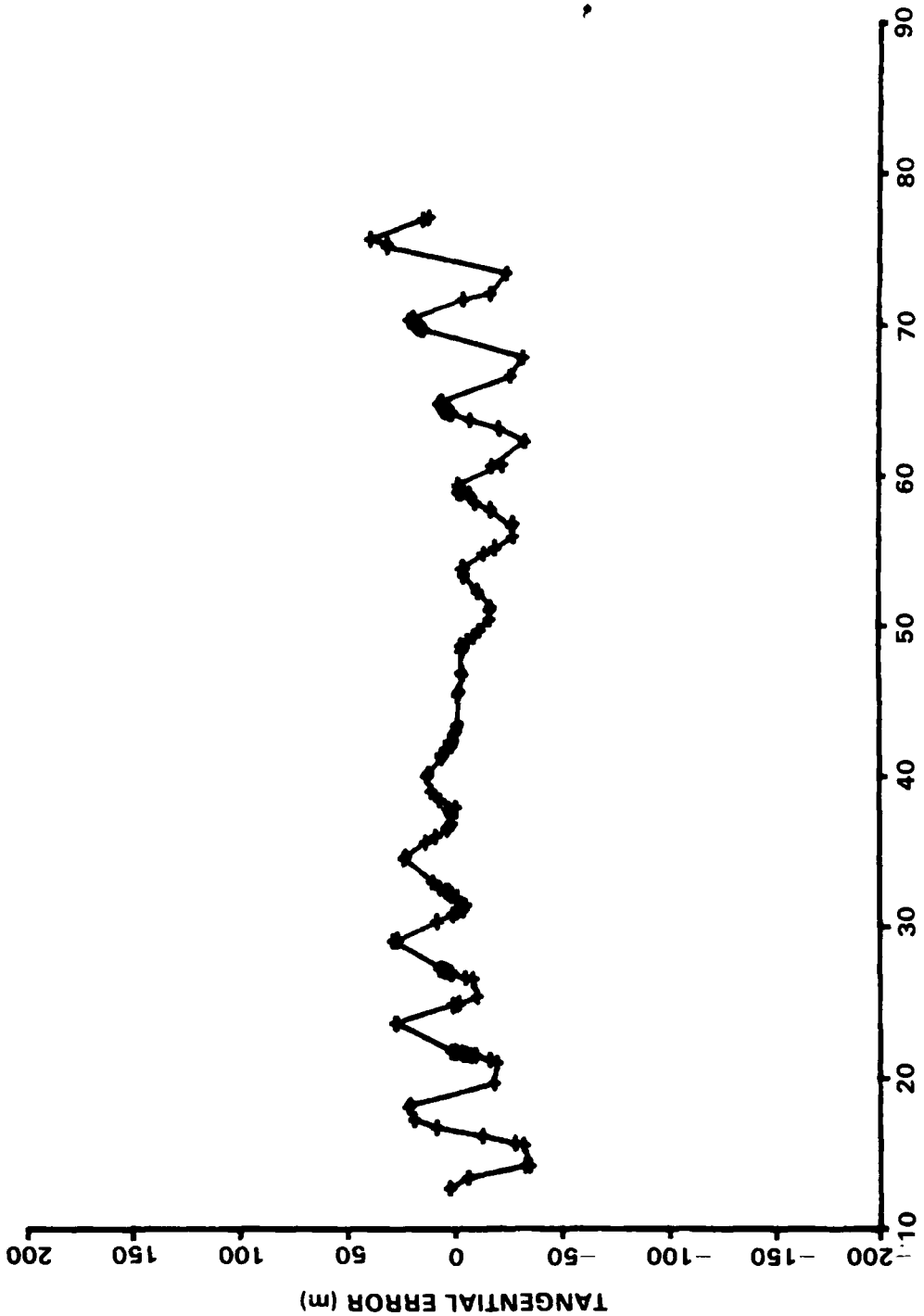

FIGURE A-3. 25 x 25 GRAVITY FIELD SEA MODEL ATMOSPHERE SINGLE DRAG SEGMENT

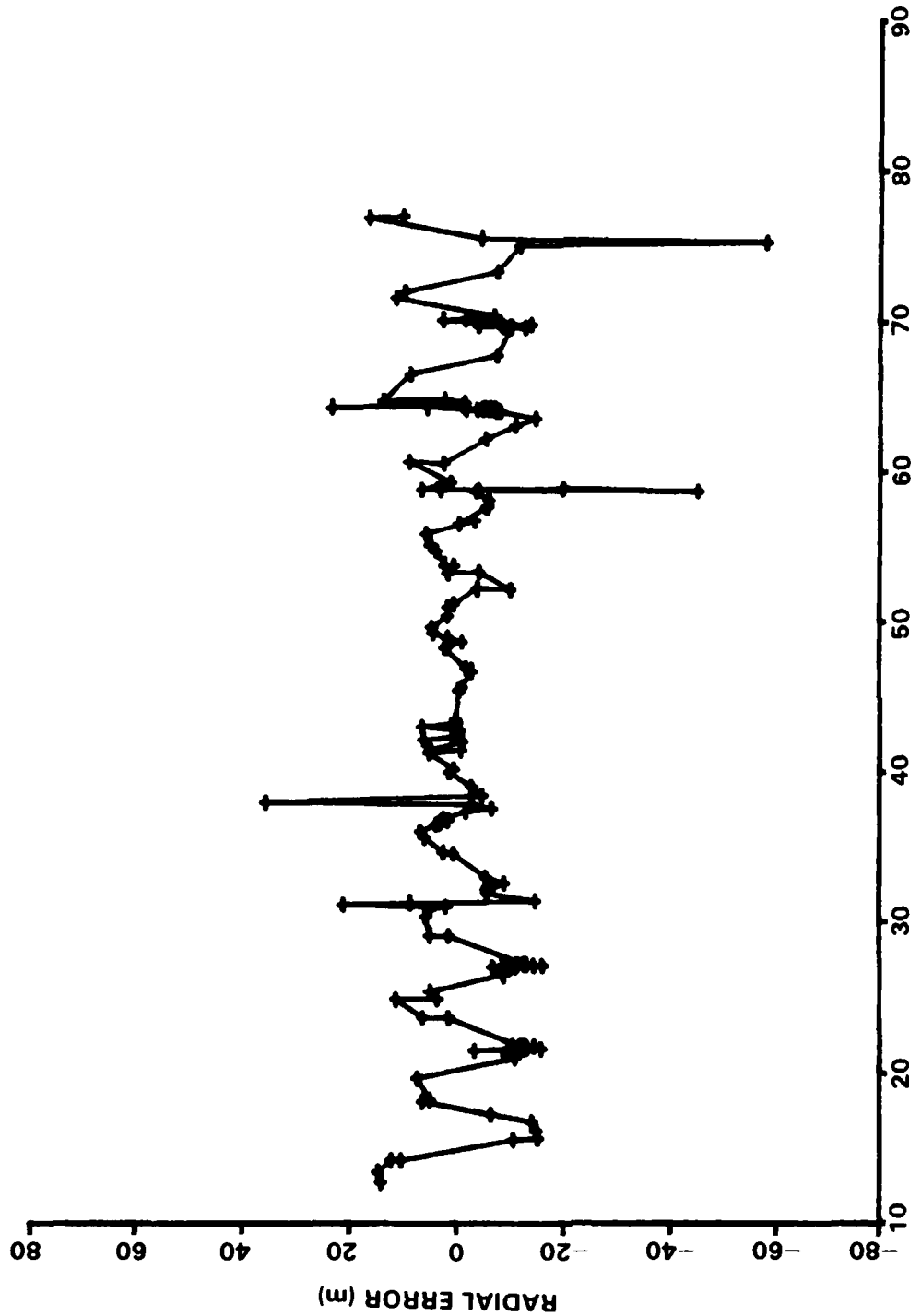

FIGURE A-4. 25 x 25 GRAVITY FIELD SEA MODEL ATMOSPHERE SINGLE DRAG SEGMENT

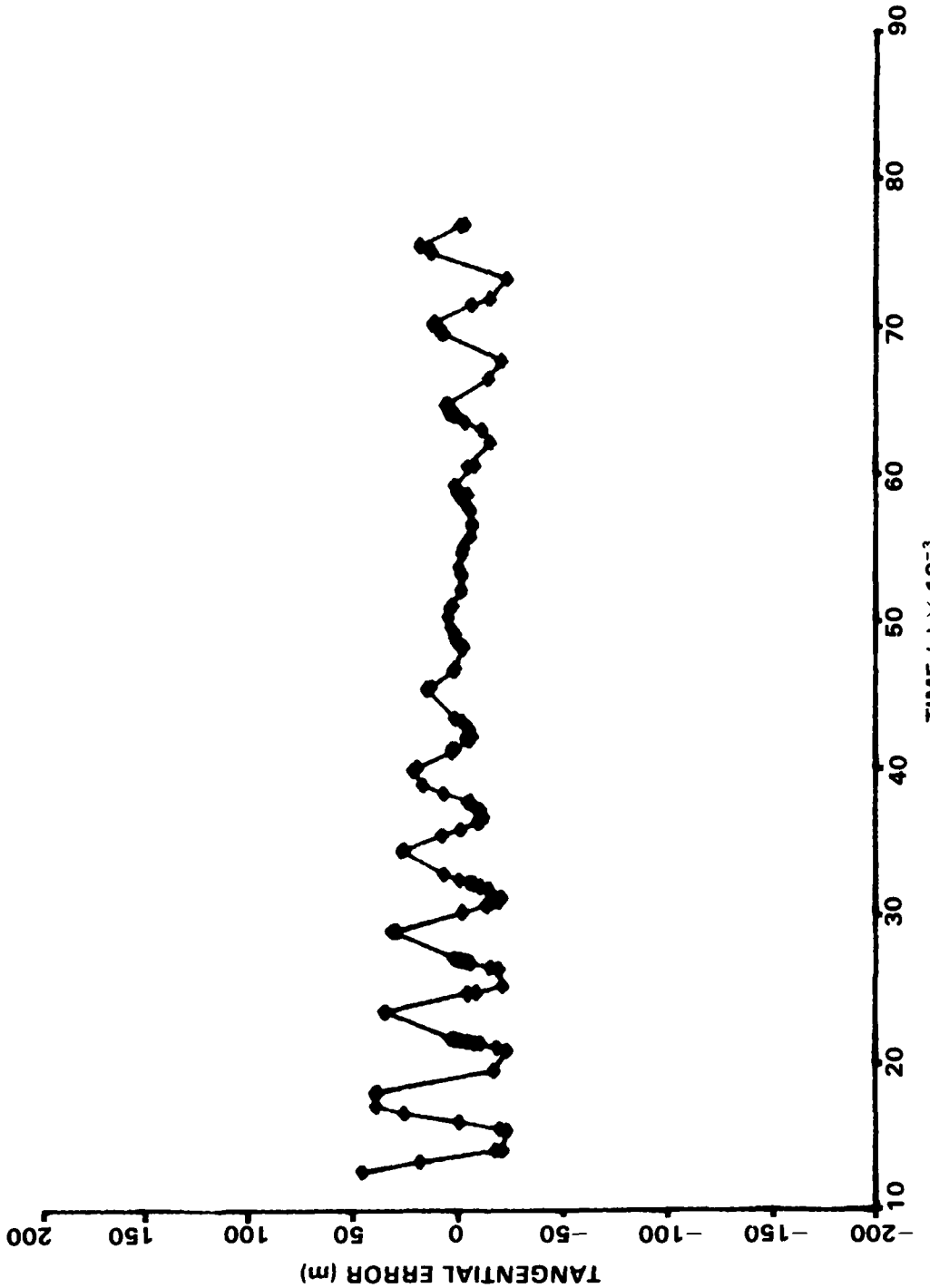

FIGURE A-5. 25 x 25 GRAVITY FIELD SEA MODEL ATMOSPHERE 4 DRAG SEGMENTS

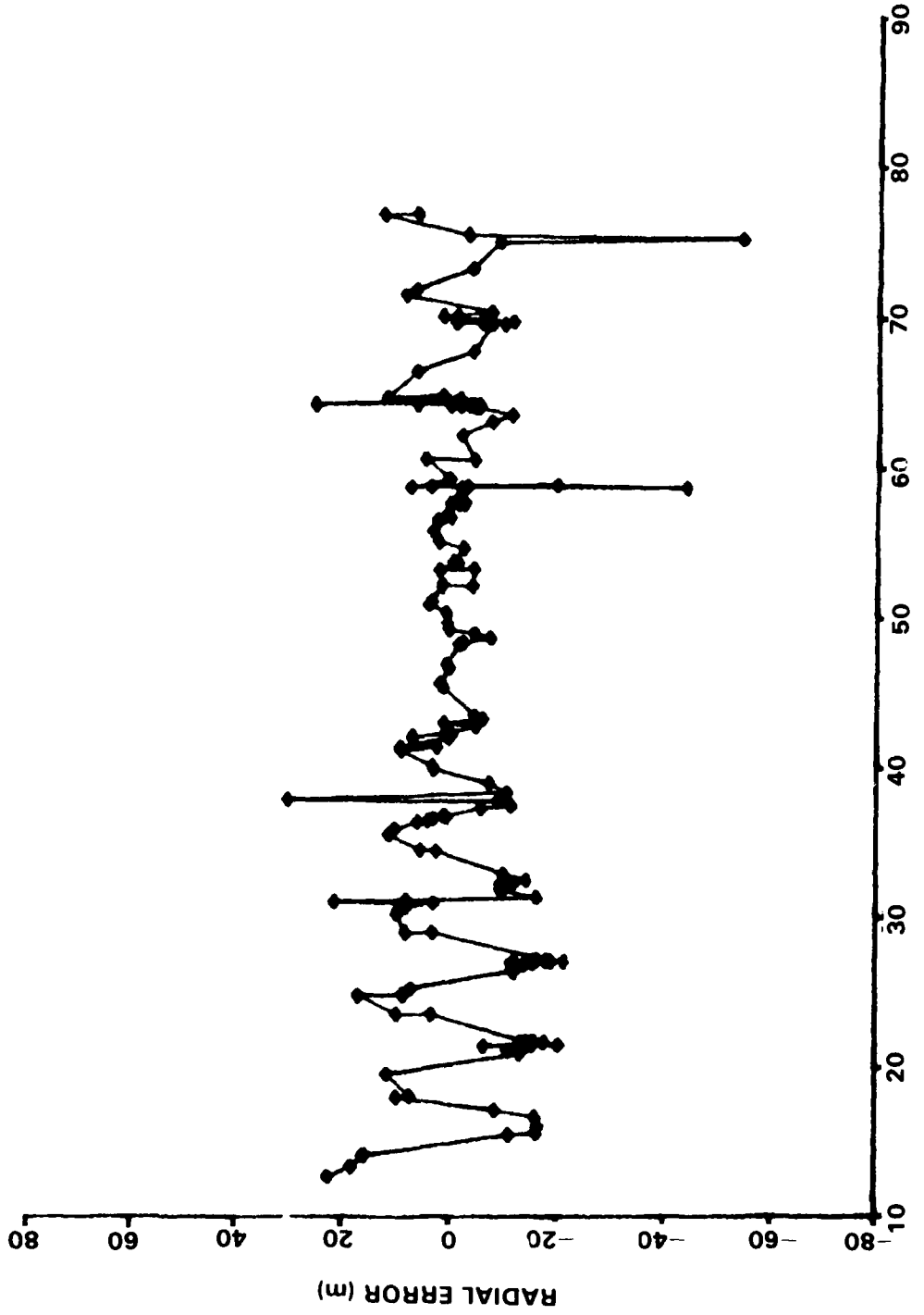

FIGURE A-6. 25 x 25 GRAVITY FIELD SEA MODEL ATMOSPHERE 4 DRAG SEGMENTS

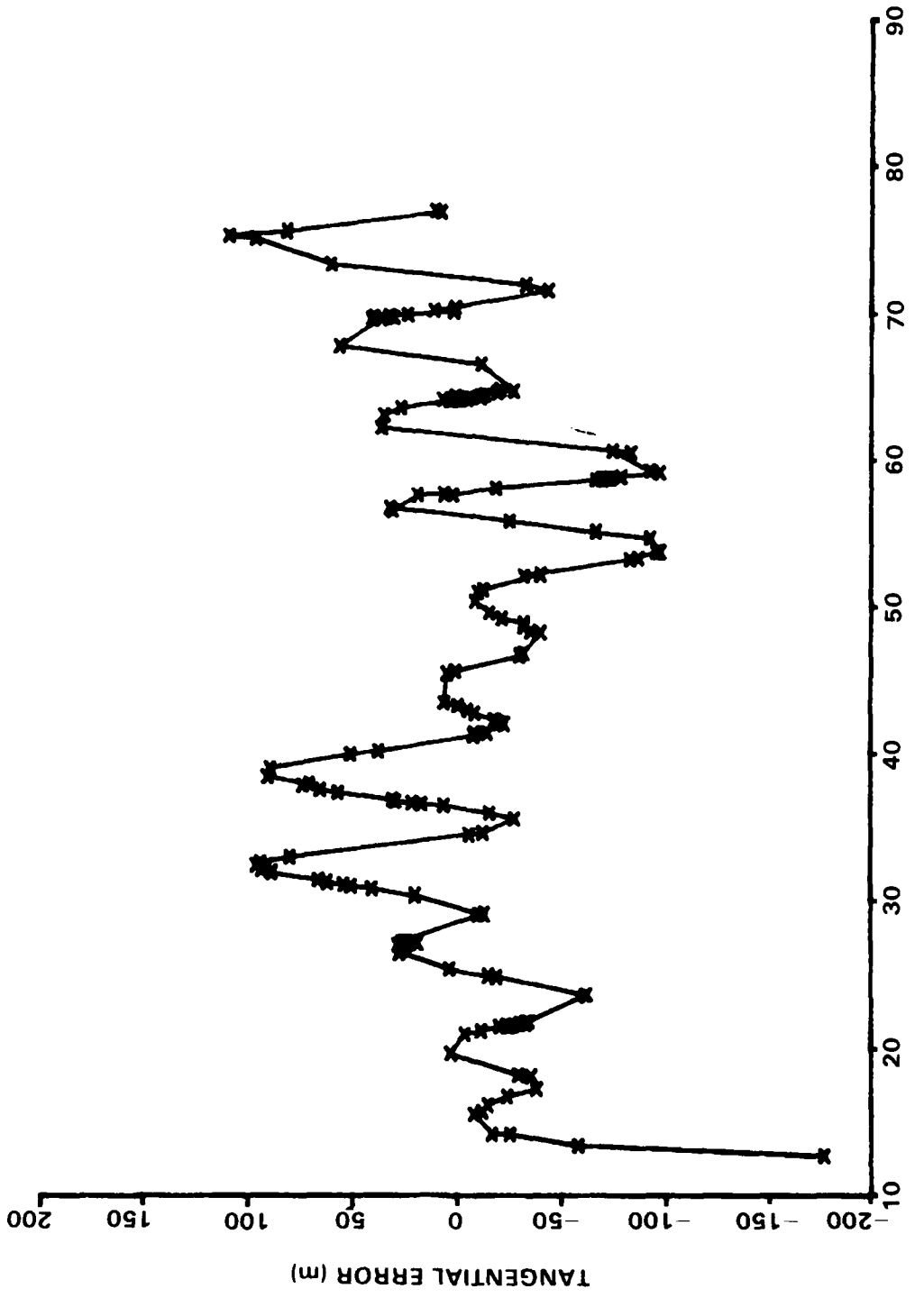

FIGURE A-7. 14 x 14 GRAVITY FIELD MJB MODEL ATMOSPHERE SINGLE DRAG SEGMENT

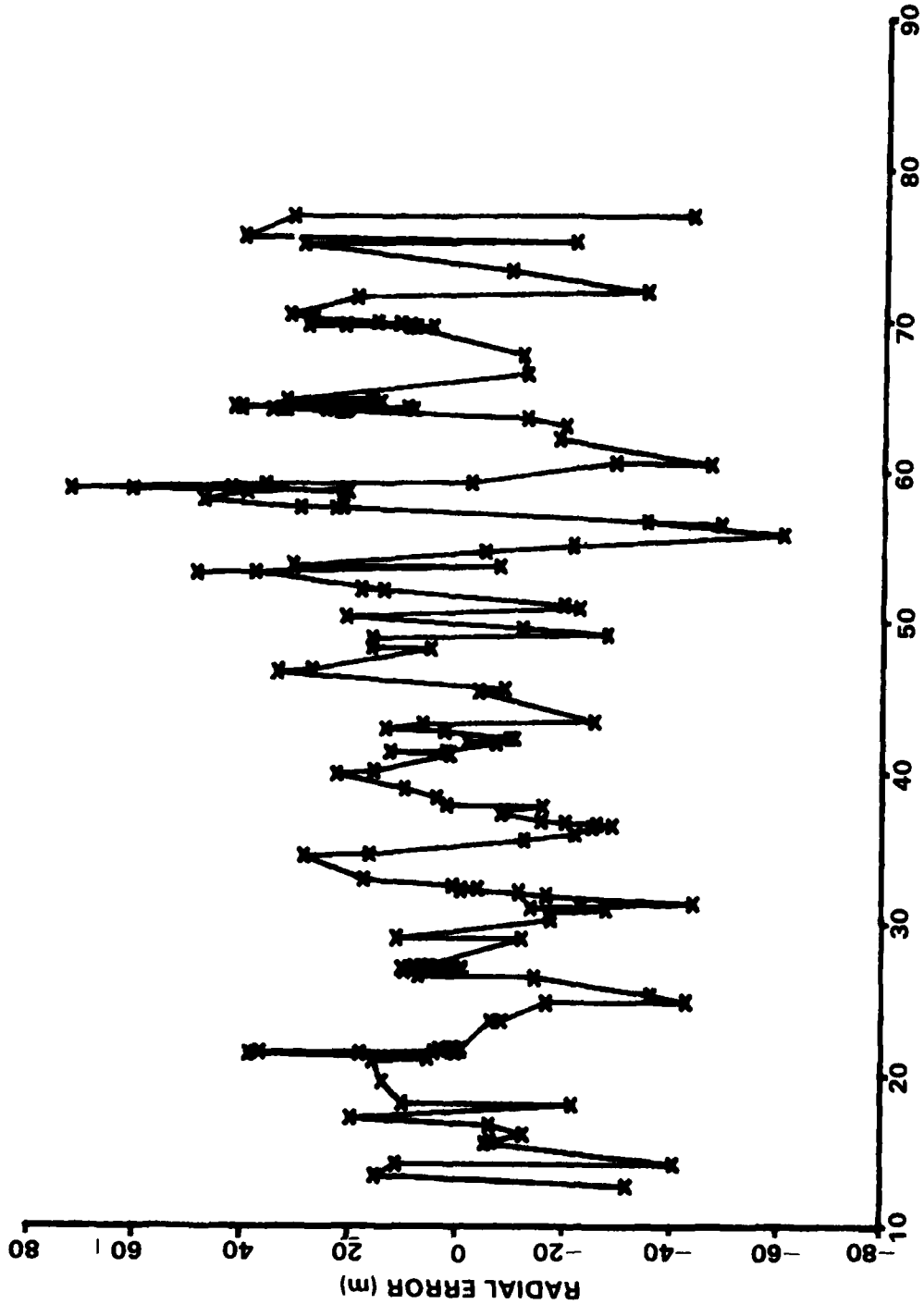

FIGURE A-8. 14 x 14 GRAVITY FIELD MJB MODEL ATMOSPHERE SINGLE DRAG SEGMENT

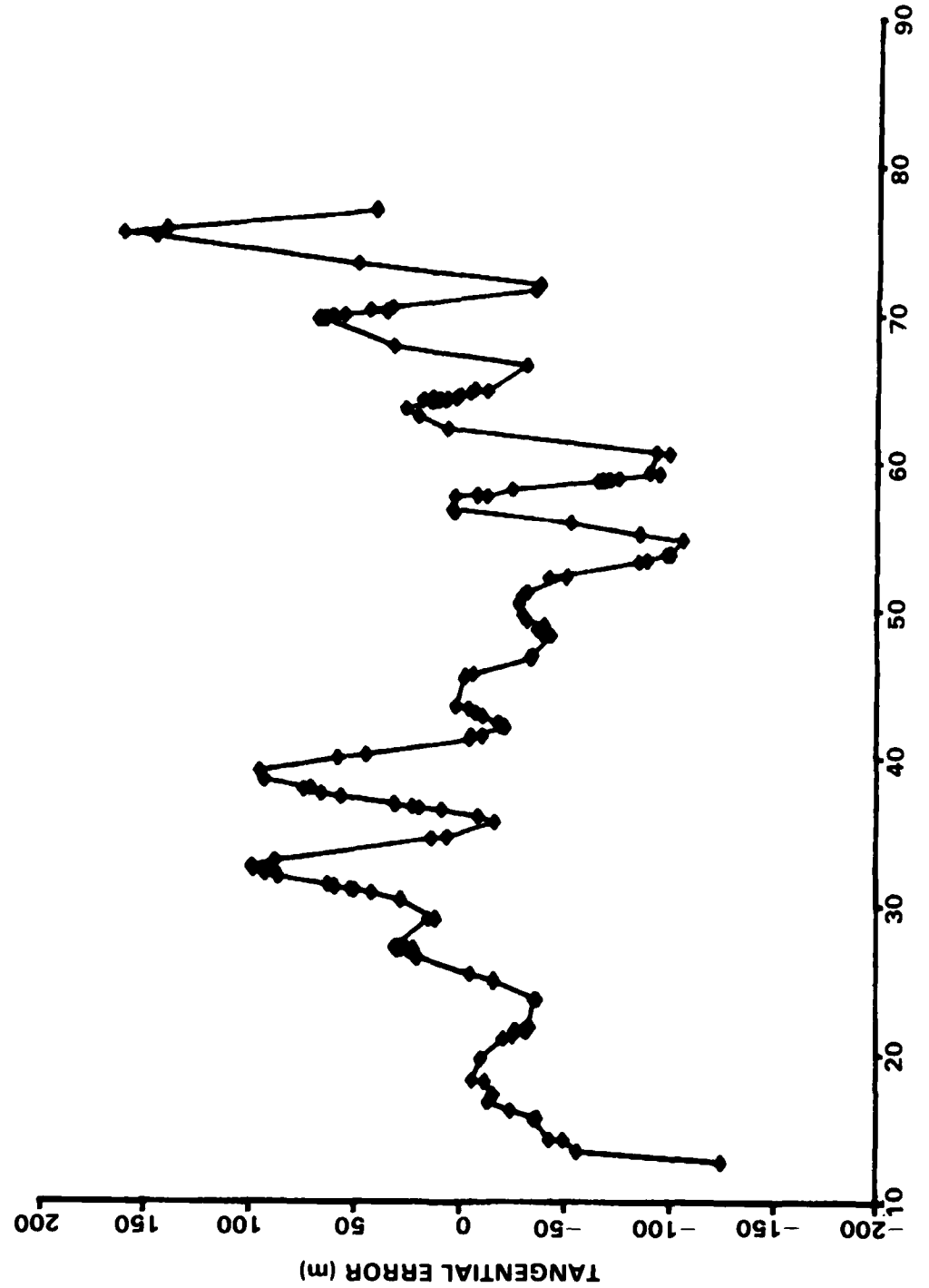

FIGURE A-9. 14 x 14 GRAVITY FIELD SEA MODEL ATMOSPHERE SINGLE DRAG SEGMENT

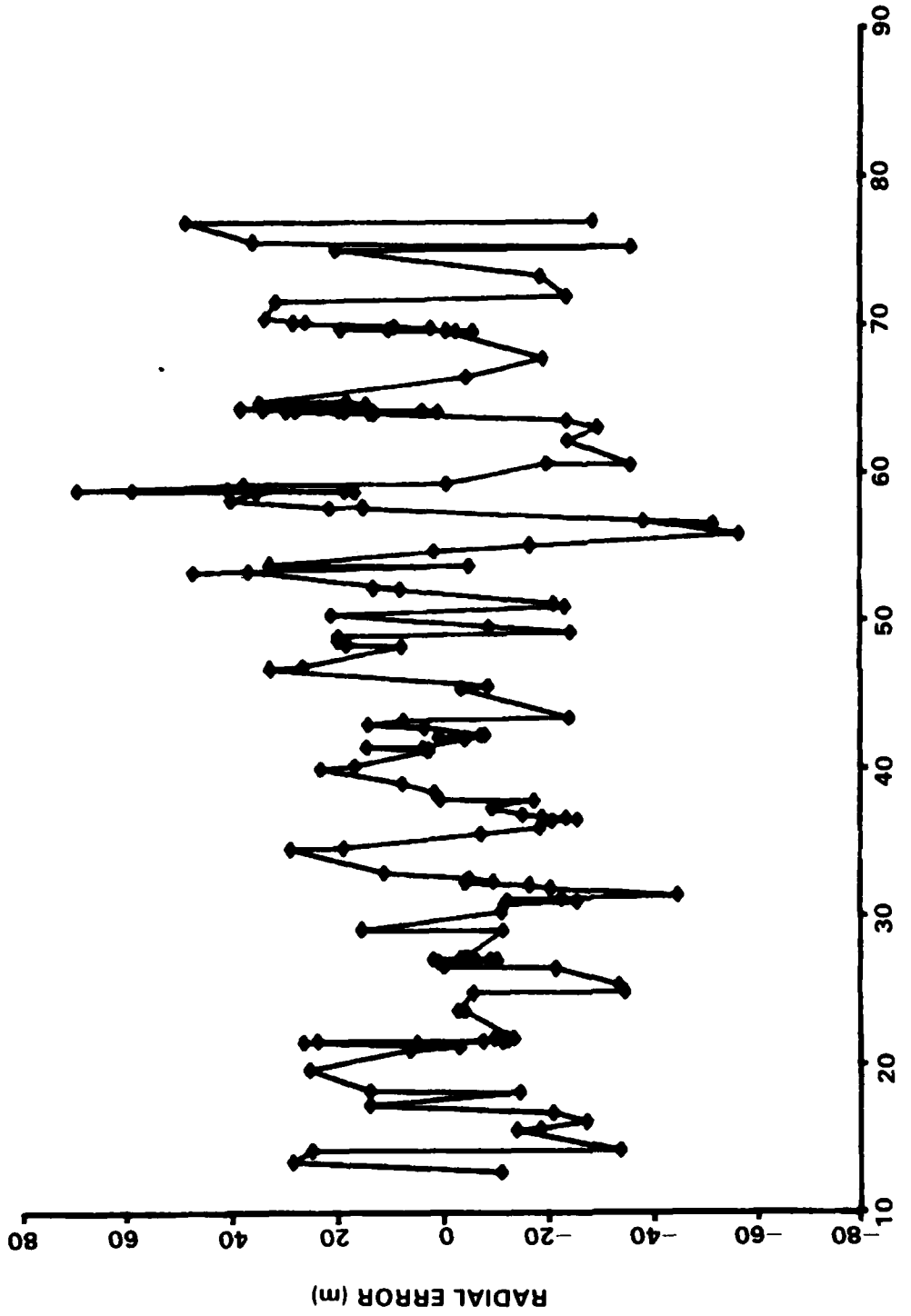

FIGURE A-10. 14 x 14 GRAVITY FIELD SEA MODEL ATMOSPHERE SINGLE DRAG SEGMENT

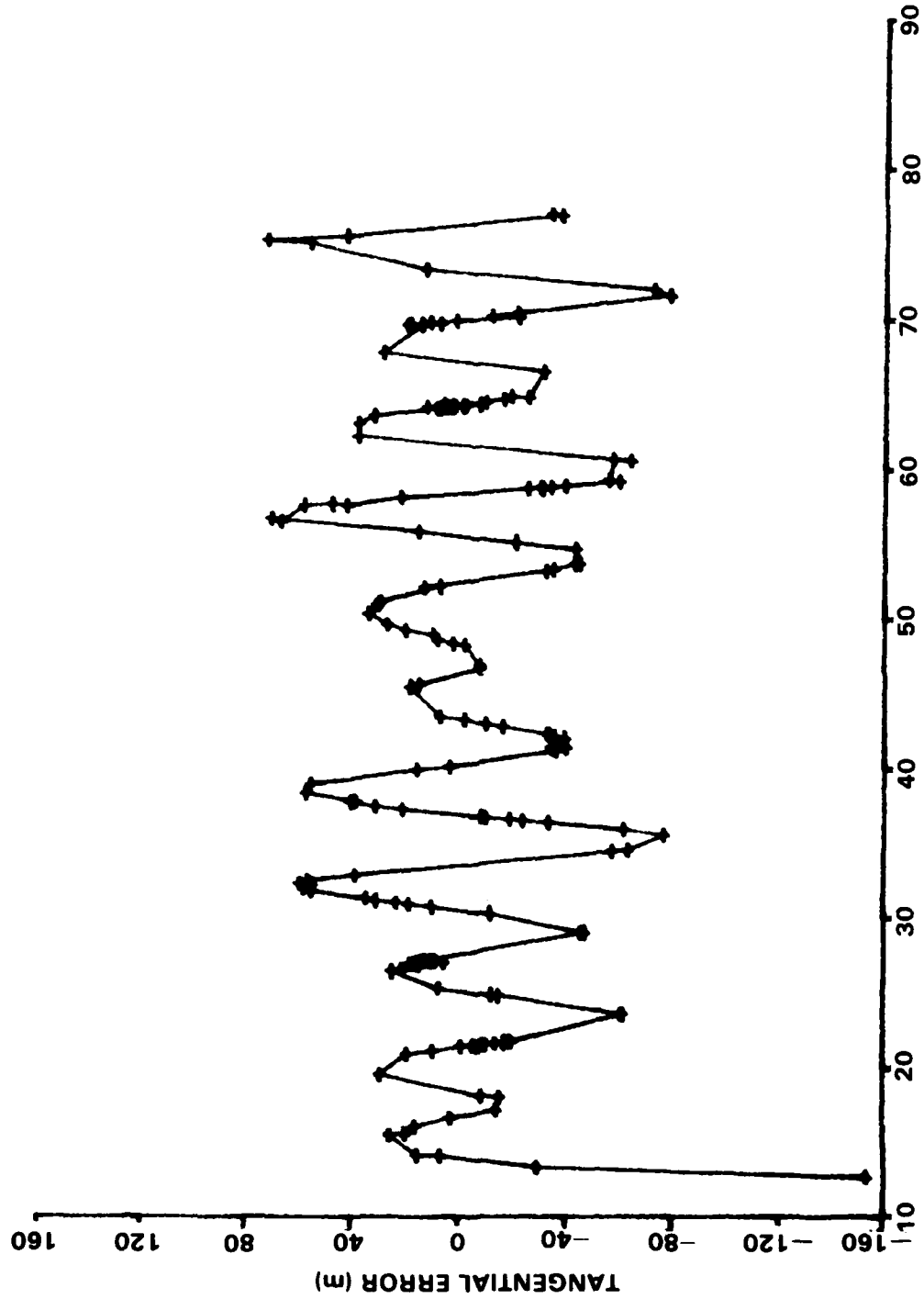

FIGURE A-11. 14 x 14 GRAVITY FIELD MJB MODEL ATMOSPHERE 4 DRAG SEGMENTS

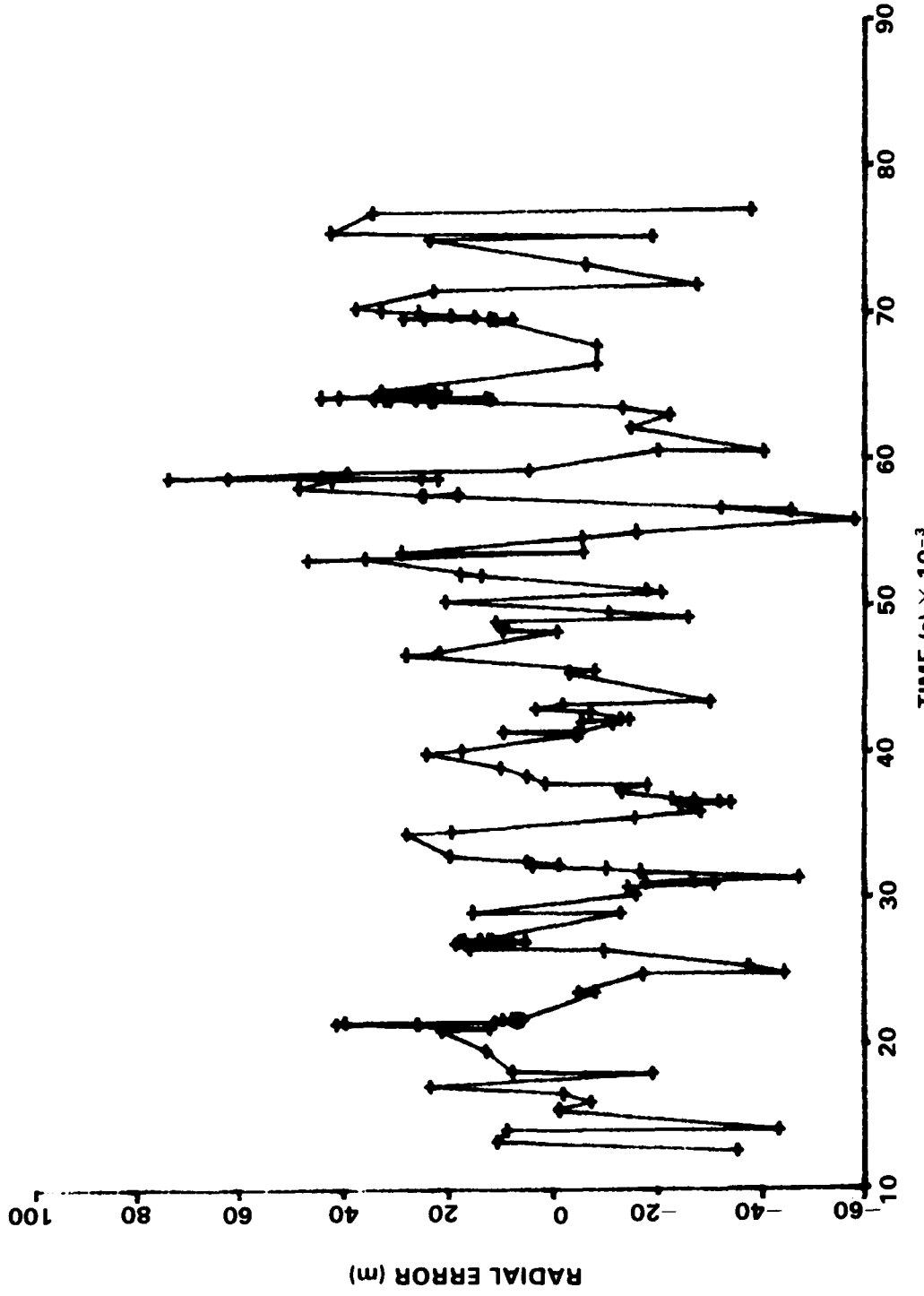

FIGURE A-12. 14 x 14 GRAVITY FIELD MJB MODEL ATMOSPHERE 4 DRAG SEGMENTS

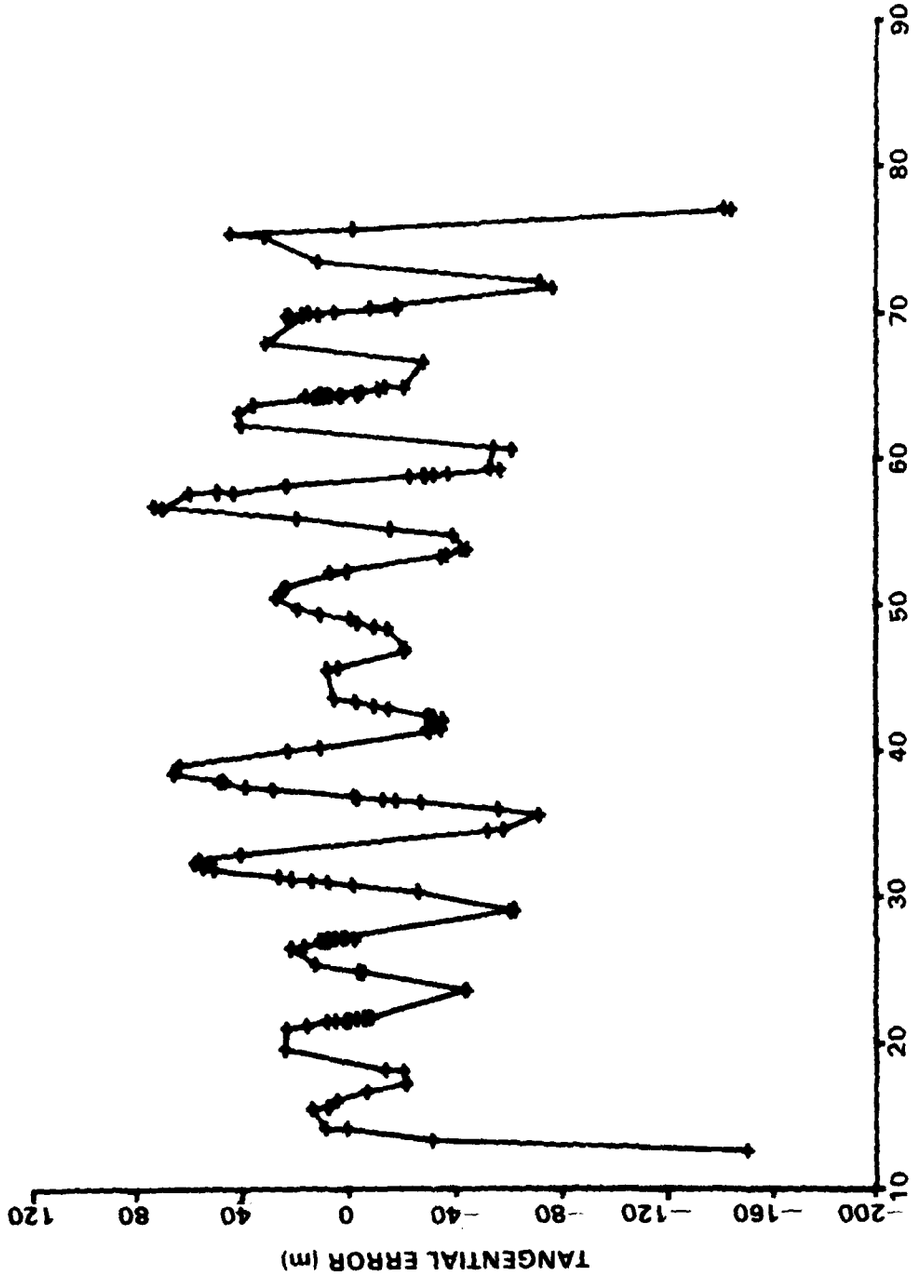

FIGURE A-13. 14 x 14 GRAVITY FIELD MJB MODEL ATMOSPHERE 10 DRAG SEGMENTS

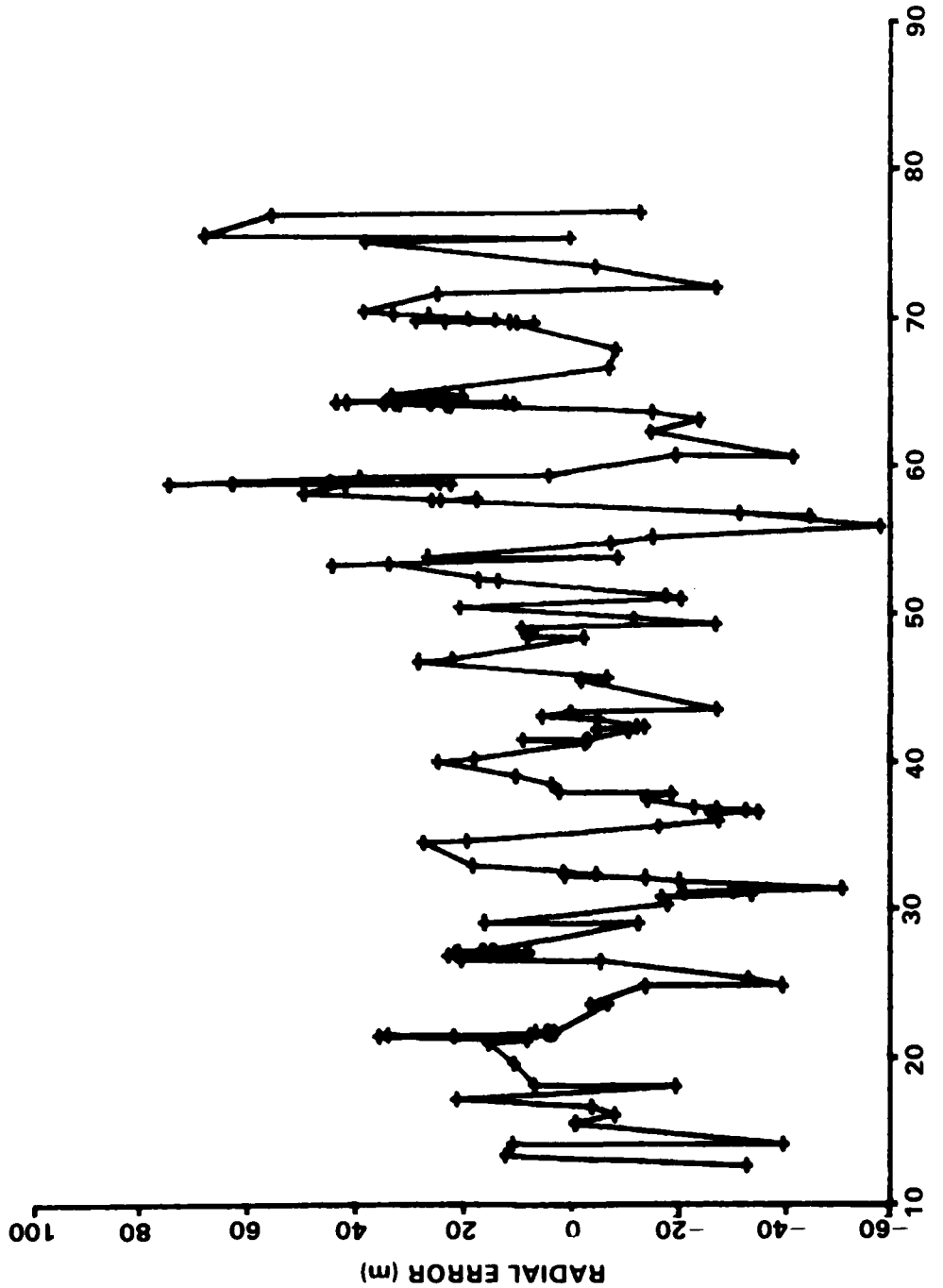

FIGURE A-14. 14 x 14 GRAVITY FIELD MJB MODEL ATMOSPHERE 10 DRAG SEGMENTS

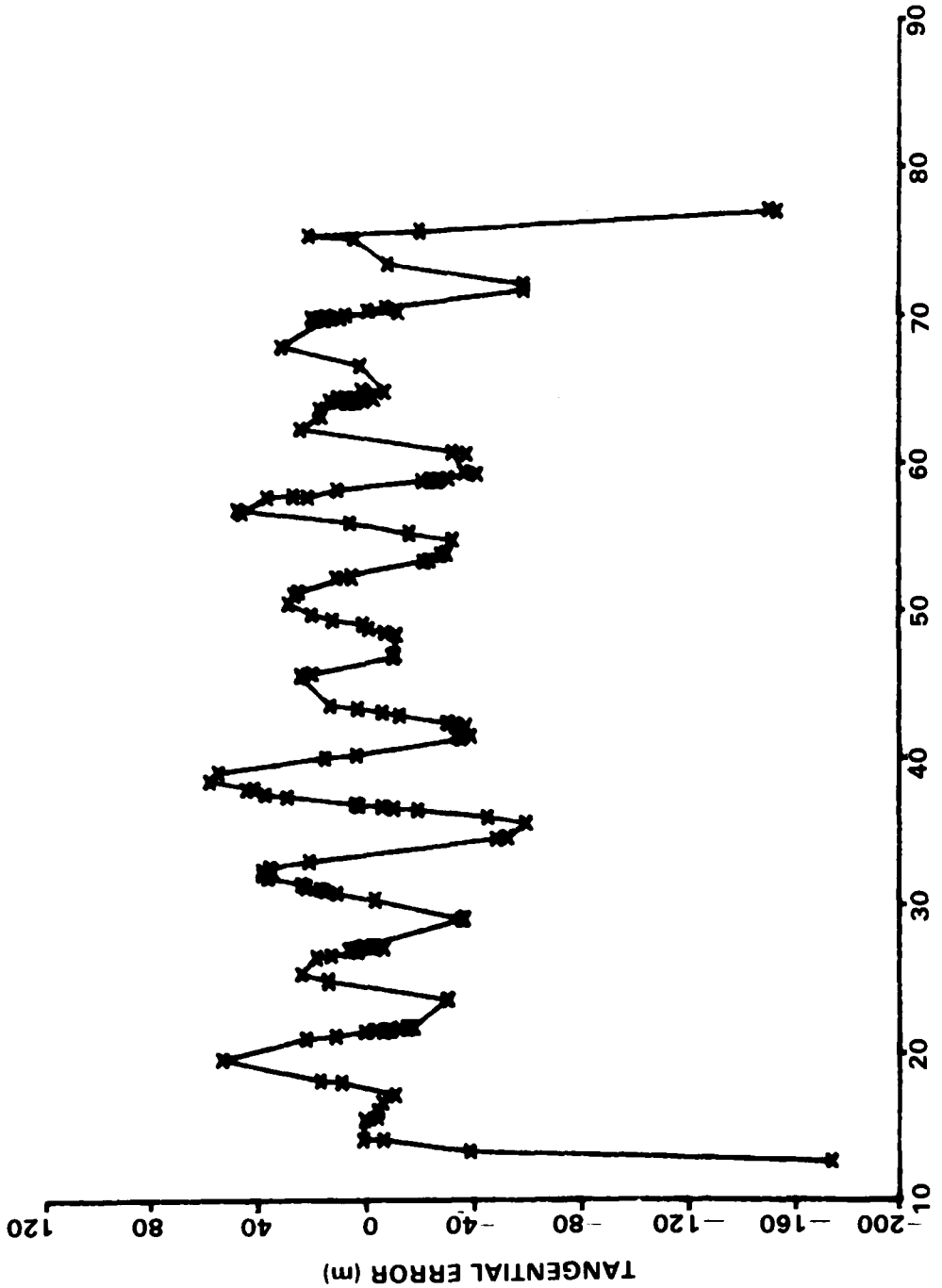

FIGURE A-15. 14 x 14 GRAVITY FIELD MJB MODEL ATMOSPHERE 20 DRAG SEGMENTS

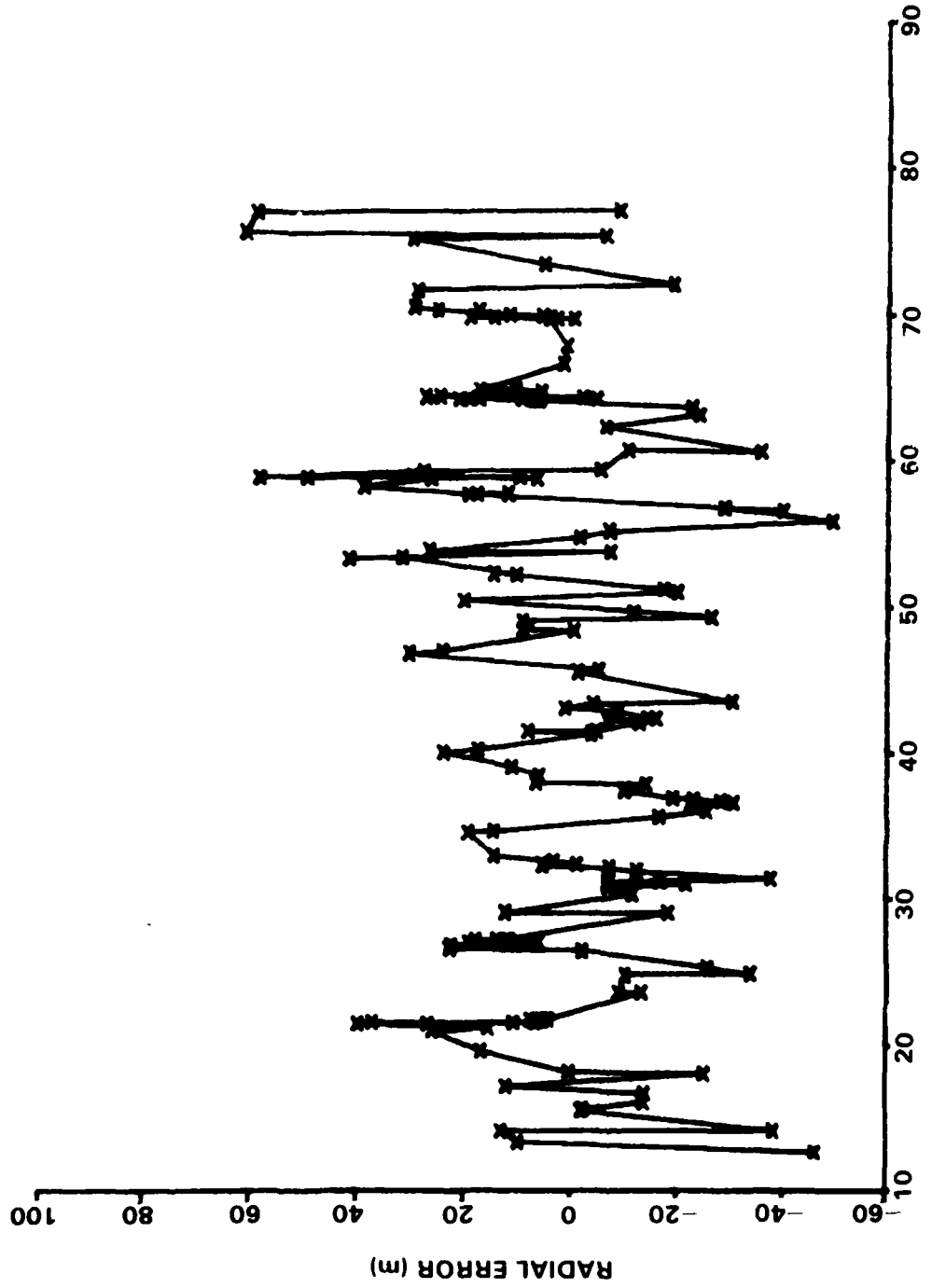

FIGURE A-16. 14 x 14 GRAVITY FIELD MJB MODEL ATMOSPHERE 20 DRAG SEGMENTS

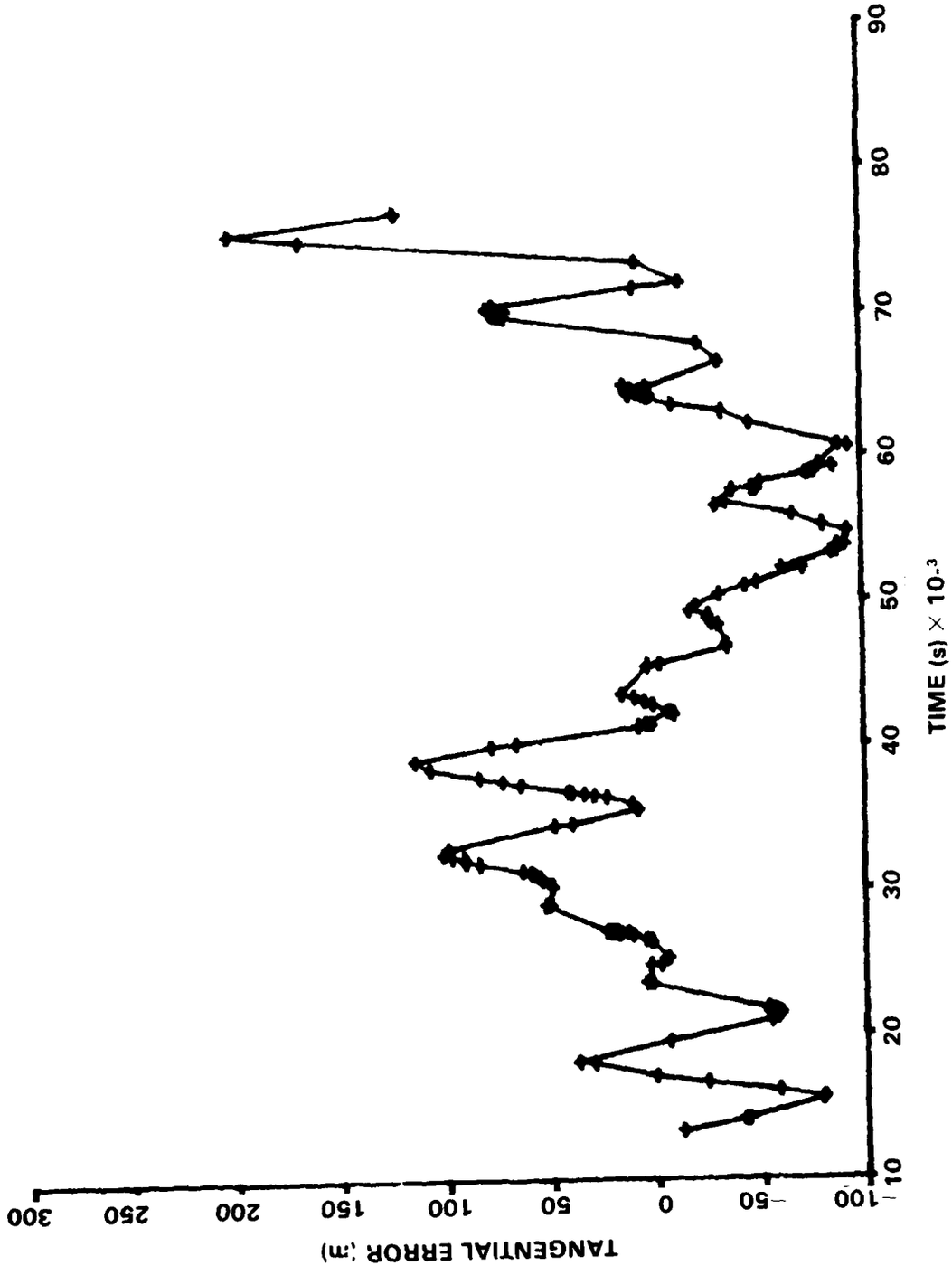

FIGURE A-17. 14 x 14 GRAVITY FIELD SEA MODEL ATMOSPHERE SINGLE DRAG SEGMENT HIGH SOLAR FLUX

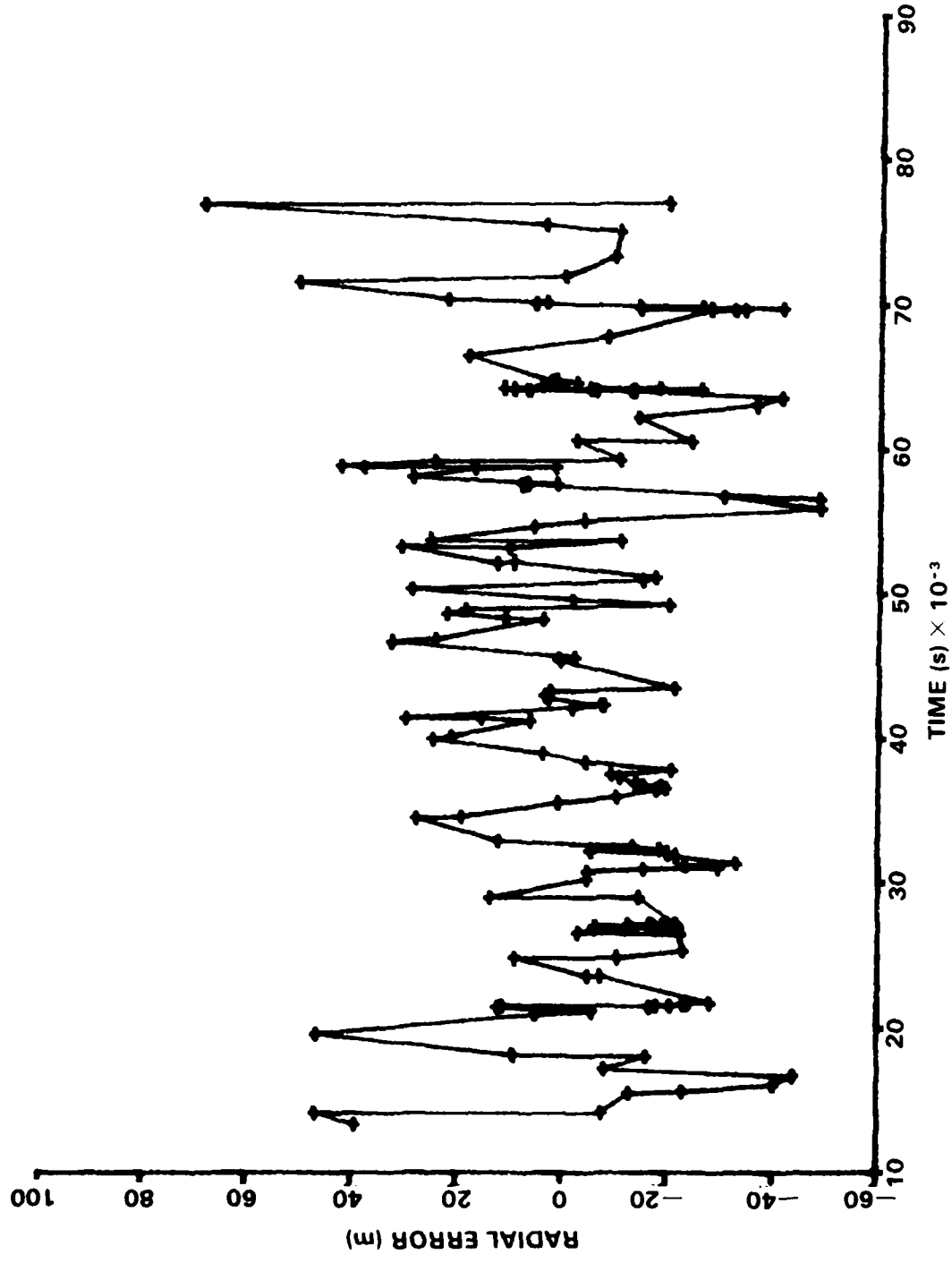

FIGURE A-18. 14 x 14 GRAVITY FIELD SEA MODEL ATMOSPHERE SINGLE DRAG SEGMENT HIGH SOLAR FLUX

DISTRIBUTION

Defense Technical Information Center
Cameron Station
Alexandria, VA 22314 (12)

Library of Congress
ATTN: Gift and Exchange Division (4)
Washington, DC 20540

National Aeronautics and Space Administration
Scientific and Technical Library
Code NHS 22, Rm. BA39
600 Independence Avenue, SW
Washington, DC 20546 (2)

Defense Mapping Agency
ATTN: Mr. Jack Calender (10)
Washington, DC 20305

Defense Mapping Agency
Hydrographic/Topographic Center
ATTN: Mr. Patrick Fell (10)
Washington, DC 20390

Defense Mapping Agency Aerospace Center
ATTN: Dr. Robert Ballew (8)
St. Louis, MO 63118

Naval Electronics Systems Command
Navy Space Project, PME106
Washington, DC 20360 (3)

Office of Naval Research
Physical Sciences Division
800 N. Quincy St. (2)
Arlington, Va 22217

Air Force Geophysics Laboratory
Hanscom Field
Bedford, MA 01731 (2)

Goddard Space Flight Center
ATTN: Dr. David Smith (1)
Greenbelt, MD 20771

The University of Texas at Austin
ATTN: Dr. Byron Tapley (1)
Austin, TX 78712

Applied Research Laboratory
University of Texas
ATTN: Dr. Arnold Tucker (5)
Austin, TX 78712

Physical Sciences Laboratory
New Mexico State University
Box 3 - PSL
ATTN: Dan Martin (3)
Las Cruces, NM 88003

Applied Physics Laboratory
Johns Hopkins University
Johns Hopkins Road
ATTN: Harold Black (3)
Laurel, MD 20810

DISTRIBUTION (Continued)

Office of Chief of Naval Operations
Naval Oceanography Division (NOP-952)
Bldg. 1, U.S. Naval Observatory (2)
Washington, DC 20390

Office of Naval Operations
Navy Space Systems Division
(NOP-943) (2)
Washington, DC 20350

Naval Research Laboratory
ATTN: Mr. Al Bartholomew (3)
Washington, DC 20375

Naval Oceanographic Office
Bay St Louis, MS 39522 (2)

Local:

E31 (GIDEP)
E411 (Rouse)
E431 (10)
F14 (4)
K05 (2)
K12 (10)
K13 (20)
K14 (5)